Stigmergic construction and topochemical information shape ant nest architecture

Anais Khuong, Jacques Gautrais, Andrea Perna, Chaker Sbai, Maud Combe, Pascale Kuntz, Christian Jost, Guy Theraulaz

Stigmergic construction and topochemical information shape ant nest architecture

Anaïs Khuong[a,b], Jacques Gautrais[a,b], Andrea Perna[a,b,1], Chaker Sbaï[a,b,c,d], Maud Combe[a,b], Pascale Kuntz[e], Christian Jost[a,b], and Guy Theraulaz[a,b,2]

[a]Centre de Recherches sur la Cognition Animale, Centre de Biologie Intégrative (CBI), Centre National de la Recherche Scientifique (CNRS), Université Paul Sabatier (UPS), F-31062 Toulouse Cedex 9, France; [b]CNRS, Centre de Recherches sur la Cognition Animale, F-31062 Toulouse, France; [c]Institut de Mathématiques de Toulouse, Université Paul Sabatier, Institut National des Sciences Appliquées, Université Toulouse 1 Capitole, Université Toulouse II Le Mirail, F-31062 Toulouse, France; [d]Institut de Mathématiques de Toulouse, UMR 5219, CNRS, F-31062 Toulouse, France; and [e]Laboratoire d'Informatique de Nantes Atlantique, Polytech'Nantes, 44300 Nantes, France

Edited by William Bialek, Princeton University, Princeton, NJ, and approved December 4, 2015 (received for review May 19, 2015)

The nests of social insects are not only impressive because of their sheer complexity but also because they are built from individuals whose work is not centrally coordinated. A key question is how groups of insects coordinate their building actions. Here, we use a combination of experimental and modeling approaches to investigate nest construction in the ant *Lasius niger*. We quantify the construction dynamics and the 3D structures built by ants. Then, we characterize individual behaviors and the interactions of ants with the structures they build. We show that two main interactions are involved in the coordination of building actions: (*i*) a stigmergic-based interaction that controls the amplification of depositions at some locations and is attributable to a pheromone added by ants to the building material; and (*ii*) a template-based interaction in which ants use their body size as a cue to control the height at which they start to build a roof from existing pillars. We then develop a 3D stochastic model based on these individual behaviors to analyze the effect of pheromone presence and strength on construction dynamics. We show that the model can quantitatively reproduce key features of construction dynamics, including a large-scale pattern of regularly spaced pillars, the formation and merging of caps over the pillars, and the remodeling of built structures. Finally, our model suggests that the lifetime of the pheromone is a highly influential parameter that controls the growth and form of nest architecture.

collective animal behavior | stigmergy | ants | nest building | computational modeling

Insect societies, such as ants and termites, are among the living organisms that build the most diverse and complex forms of nests (1–4). These nests play a crucial role in the growth and adaptation of colonies: the nests ensure a protection against predation, provide a place to store food, and allow an efficient regulation of energy and gas exchanges with the outside environment (5–10). Within termite nests, intricate communication pathways create efficient and robust networks connecting the various areas of a nest (11, 12). Even more remarkable is the ability of social insects to reshape their nests when colony size is growing or when environmental conditions such as temperature, moisture, and light are changing (13, 14). One fundamental question is: How are these efficient and plastic structures built? How do insects communicate and coordinate millions of building actions in such a way that the resulting nest's shape copes with external conditions? Since the pioneering work by P. P. Grassé, who introduced the concept of "stigmergy" (15), very few studies have addressed these questions and fewer have provided an experimental validation of stigmergic interactions. The underlying principle of stigmergy is that by modifying the local environment, an insect can indirectly influence the actions of other insects of the same colony at a later time, thereby leading to the emergence of coordinated collective behavior (16). Theoretical models have been proposed to account for 3D nest construction in wasps and termites (17–19), indicating that stigmergic interactions can potentially explain the coordination of nest building in these animal groups. However, a detailed and experimentally founded understanding of the interactions between the animals and the structures that they are building is limited to the construction of simple 2D structures produced by ants and termites, either by digging the substrate (20–25) or piling soil particles (26–28). In ants, 3D nest construction remains poorly documented and so far no study has attempted to connect a detailed quantitative description of individual building behavior with the growth dynamics and the resulting shape of nests.

Understanding construction behavior in social insects is a challenging task because of the difficulty to gain access to workers' activities within a nest. Here, we use a combination of experimental and modeling approaches to investigate the 3D nest construction in the ant *Lasius niger*. This ant species, in addition to digging underground galleries through the soil, frequently also assembles soil particles, to build small mounds and other structures in natural soil cavities or in the meadows (29). We aim at disentangling the coordination mechanisms in the early building stage, when the first pillars or walls emerge (within 2–7 d). We first analyze the 3D structure of *L. niger* nests from X-ray tomography. We then focus on the construction dynamics at two different scales: (*i*) the behaviors of individual workers and (*ii*) the resulting collective patterns. We use a simplified setup in which we control the amount of available building material

Significance

Social insects build some of the most complex nests found in the animal kingdom. Here, we use experiments and modeling to decipher the mechanisms involved in the coordination of nest building in the ant *Lasius niger*: we first characterize nest architecture and its growth with 3D imaging techniques; then, we test the building responses of individual ants to artificial stimuli. A model entirely based on experimental data confirms that the individual level interactions and building rules are sufficient to reproduce the nest growth dynamics and the spatial patterns observed for real ant nests. Our results show that a pheromone added by ants to the building material is a key factor that controls the growth and form of nest architecture.

Author contributions: G.T. designed research; A.K. and J.G. developed the 3D model; A.K., A.P., C.S., C.J., and G.T. performed research; M.C. and P.K. contributed new reagents/analytic tools; A.K., J.G., A.P., C.S., M.C., P.K., C.J., and G.T. analyzed data; and J.G., C.J., and G.T. wrote the paper.

The authors declare no conflict of interest.

This article is a PNAS Direct Submission.

Freely available online through the PNAS open access option.

[1]Present address: Unit of Social Ecology, Université Libre de Bruxelles, 1050 Bruxelles, Belgium.

[2]To whom correspondence should be addressed. Email: guy.theraulaz@univ-tlse3.fr.

This article contains supporting information online at www.pnas.org/lookup/suppl/doi:10.1073/pnas.1509829113/-/DCSupplemental.

and we record and quantify at regular time intervals the 3D structures built by groups of ant workers. With a separate set of experiments, we also quantify individual building behaviors and the interactions of ants with the structures that they build. We then use these data to build and calibrate a 3D stochastic model of collective construction behavior. The model allows us to analyze our experimental results and reveals that a pheromone added by ants to the building material is a key factor responsible for the observed spatial patterns. Because of its limited lifetime, this pheromone is not homogeneously present on the surface of the built structures, thus creating a topochemical landscape that determines the places at which ants concentrate their building activity. The pheromone thus controls the growth dynamics and the resulting nest architecture.

Results

Quantitative Description of Nest Structure. To compare the structures built by ants in laboratory settings with the nests constructed in the field, we collected two *L. niger* mounds built in natural conditions from meadows (Fig. 1*A*). The mounds were imaged with X-ray CT and reconstructed into 3D digital images (Fig. 1*B* and *SI Materials and Methods*). The internal structure of the nest is composed of a large number of interconnected chambers and galleries. The volume of nest A (Fig. 1*A*) was 5,390 cm^3, and the volume of nest B was 7,099 cm^3. In both nests, the chambers and galleries occupied around 30% of the total nest volume (1,730 cm^3 for nest A and 2,134 cm^3 for nest B). Fig. S1 reports the distribution of height of all of the chambers and galleries in the nests. The peak of the distribution is at 5.9 mm for nest A and 5.5 mm for nest B. The distribution of the chambers and galleries widths is given in Fig. S2 for the two nests. For both nests, the distribution of widths is centered around 12 mm.

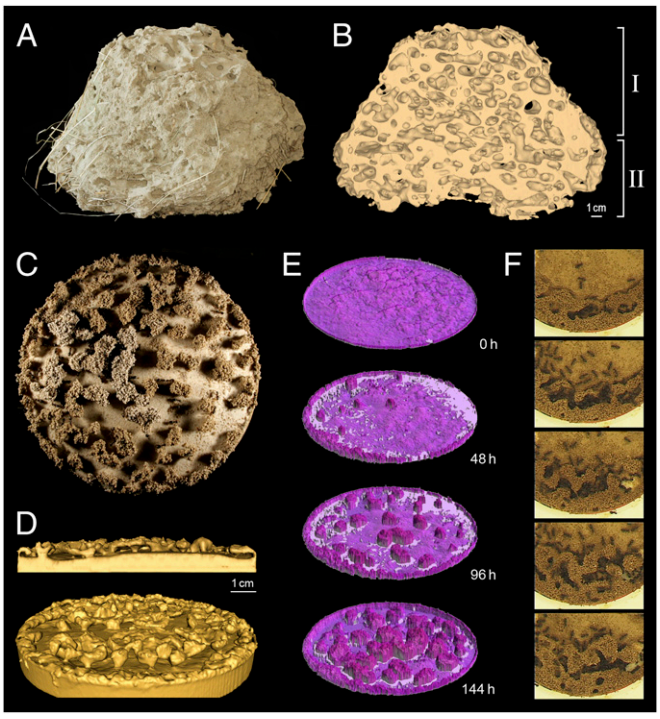

Fig. 1. (*A*) Picture of a *L. niger* field ant nest; epigeous part (I); hypogeous part (II). (*B*) Tomographic cut of the same nest. (*C*) Spatial distribution of pillars built by a group of 500 workers of the ant *L. niger* over 96 h in one experiment focusing on the first building stages. (*D*) X-ray CT scan reconstructions of the built structures (*Upper*, sagittal cut; *Lower*, side view). Note the lateral expansion of caps over the pillars. (*E*) Construction dynamics and 3D image reconstruction of the built structures from laser surface scanner data. (*F*) Image sequence showing the remodeling activity of ants over a period of 48 h.

Construction Dynamics. To quantify the collective construction dynamics and the resulting structures, groups of 500 ants were given access to a Petri dish covered with a thin layer of moistened building material (a 3-mm-high mixture of sand and clay; *SI Materials and Methods* and Fig. S3). Within a few hours after the ants' introduction, they start to build pillars reaching an average density of 0.3 pillars per cm^2 after 48 h (Figs. 1 *C* and *E* and 2*A*, Fig. S4*A*, and Movies S1 and S2). Pillars are regularly spaced with an average distance of 9.93 ± 0.66 mm (mean ± SD) between the nearest pillars, suggesting their spacing is regulated to a characteristic scale (Fig. 2 *B*, *D*, and *E*). These values of interpillar distance are comparable in scale to the values of chamber and gallery widths in the nests collected in the field. When pillars reach a critical size corresponding to a mean height of about 4 mm, ants start to build a roof by adding pieces of material on the sides of the pillars, thus rapidly increasing the surface over which the material can be dropped (Fig. 2*C*). These upper portions of pillars, called caps, have first a globular shape and then the caps' edges become flatter with time (Fig. 1*D*). It may happen that, while extending over the pillars, nearby caps come into contact, merge, and form arches that cover passages between pillars (Fig. S4 *B* and *C*). However, the limited amount of sand–clay mixture in our study prevented the ants from building a closed roof over the pillars. It is also important to notice that the shape of caps changed over time, mainly as a result of a constant remodeling activity performed by ants (Fig. 1*F*).

Individual Behavior. To investigate the mechanisms involved in nest construction, we carried out a separate set of experiments with the aim of quantifying the building behavior of individual ants and their interactions with the structures they built. Individual's building behavior consists of three easily identified components: ants first dig, pick a small amount of material, and shape a pellet; then, they move for some distance while carrying the pellet; and, finally, they either spontaneously drop the pellet on the soil surface or add it to an existing built structure. We first analyzed how built structures modulate the way ants pick up and deposit soil pellets. Our experiments show that the deposition of building material stimulates ants to accumulate more material at the same place later on, thus creating a positive-feedback loop.

To quantify this feedback loop, we estimated the probabilities to pick up and deposit a soil pellet as a function of the number of already-deposited pellets. In the experimental setup, ants had access to an empty plastic chamber whose floor was covered with a thin flat layer of moistened plaster (Fig. S5 and *SI Materials and Methods*). Building material (wet sand–clay mixture) was provided close to the chamber's entrance, a condition that strongly stimulates the ants to bring soil pellets inside the chamber. These conditions make it possible to record every building action performed by the workers, whether it is a deposition or an extraction of a piece of building material, the ants' movements over the surface of the chamber, or the size of piles made of previously deposited pellets that the ants come into contact with (Movie S3). Over time, pellets brought by workers start to form clusters that progressively lead to the formation of small piles. Thus, the deposition of material at a certain place stimulates ants to accumulate more material at that place. The probability $P(drop|n)$ that an ant deposits a pellet on a pile of n previously deposited pellets was estimated by the ratio of the number of depositions to the total number of contacts that ants carrying a pellet had with a pile of that size. We checked that the probability to deposit a pellet was not affected by the previous contacts ants had with other piles, so that the ants' behaviors can be described by Markovian processes (*SI Materials and Methods*

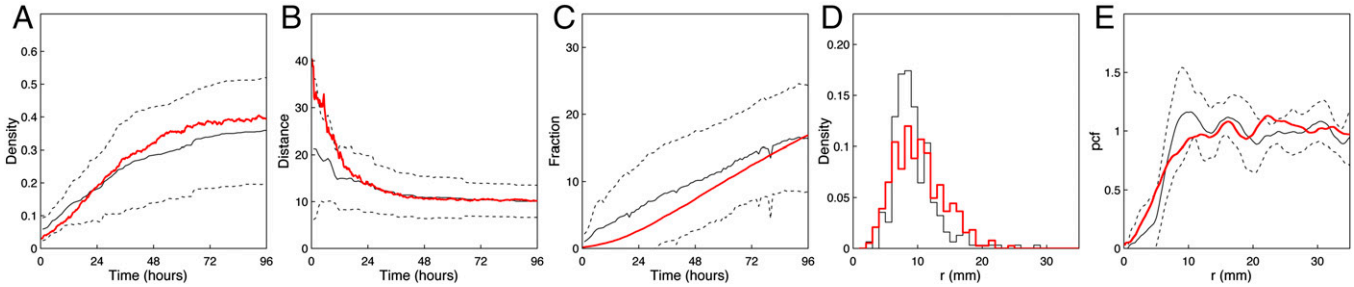

Fig. 2. Quantification of the construction dynamics. The black and dashed lines are the mean and SD of experimental data (n = 11 experiments). The red curves indicate the model predictions (over 10 simulations with a group of 500 ants and $1/\eta_{Im}$ = 1,200 s). (*A*) Dynamics of pillar density (pillar per cm^{-2}). (*B*) Dynamics of average nearest-neighbor distance between pillars (mm). (*C*) Dynamics of the fraction of surface (in %) covered by structures exceeding 3 mm (0 mm corresponds to the average height of the initial disk of construction material). (*D*) Distribution of nearest-neighbor distances between pillars after 96 h. (*E*) Pair correlation function (pcf) of the pillars' positions (derivative of the Ripley's K function, the reduced second moment function of the point process), showing a clear exclusion within the first 10 mm (pcf < 1). Beyond this distance, the locations of pillars are randomly distributed in space (pcf ≅ 1).

and Fig. S6). Fig. 3*A* suggests that $P(drop|n)$ increases with the number of previously deposited pellets.

As the number of depositions increased on the chamber's floor, we observed that ants also pick up pellets on the existing piles, thus remodeling the built structures. To determine the probability $P(pick|n)$ that an ant picks up a pellet on a pile of n previously deposited pellets, we need to estimate both the contact rate of unloaded ants with a pile of size n and the rate of change of that pile after a contact with an ant (*SI Materials and Methods*). Fig. 3*B* suggests that $P(pick|n)$ decreases with the number of previously deposited pellets (see *SI Materials and Methods* for the computation of the individual picking-up and deposition rates associated with these probabilities).

As the amount of building material already deposited in some places increases, the deposition of pellets in those places is enhanced, leading to the emergence of pillars. Then, as soon as the pillars reach some critical height, workers stop adding pellets on top of pillars and start to build extensions on the sides. To better understand this behavior, we performed an additional set of experiments in which we used artificial pillars made of wood (*SI Materials and Methods*). These pillars were about the same diameter as the ones built by ants but higher (15 mm). We measured the height at which the pellets were fastened on these pillars and found that it corresponded to the mean body length of an ant worker [Fig. 3*C*; minimum height: 4.02 ± 0.33 mm (n = 13); maximum height: 8.46 ± 0.64 mm (n = 13); mean ant body length: 4.1 ± 0.14 mm]. This result suggests that workers used their body size as a template to decide at which height they will stop to pile up pellets on an existing pillar and start to build a roof from that pillar.

We also checked whether any secretion was added to the pellets by ants during their manipulations. In termites, it has been shown that a volatile chemical substance called "cement pheromone" originating from a worker's salivary gland was added to the building material and stimulated the deposition of soil pellets (30–32). A similar pheromone might also be used by ants and could play a role in the coordination of building actions. If a chemical marking exists, it would increase an ant's rate to drop material at the sites with the most recent deposits, thus enhancing the accumulation of an increasing number of pellets. To test this hypothesis, we performed a series of experiments in which we analyzed the behavior of ants when they came into contact with two pillars: one control pillar made with fresh building material that had never been in contact with ants and one with material that had been recently manipulated by ants (*SI Materials and Methods*). Fig. 3*D* shows that within a few minutes after the ants' introduction in the experimental arena, there was a highly significant proportion of ants in a circular area of 6 cm^2 around the pillar made with freshly manipulated material in comparison with the same area around the control pillar. These results clearly reveal the existence of a chemical compound in the material manipulated by ants that has a retention effect on the ants. This effect, which has recently been described in termites (33), may concentrate workers carrying pellets in some locations and hence lead to a concentration of depositions at

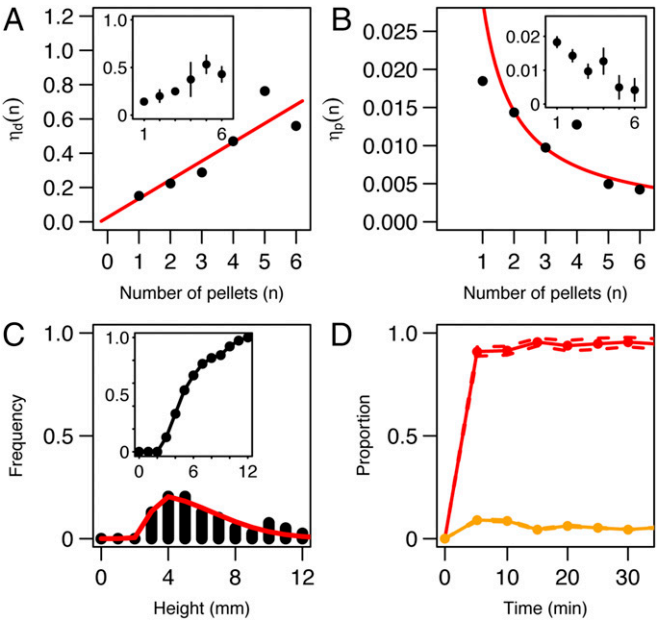

Fig. 3. Quantification of individual behavior. (*A* and *B*) The rates of deposition $\eta_d(n)$ of (*A*) and picking up $\eta_p(n)$ (*B*) a pellet as a function of the number of deposited pellets (solid dots) and the fitted parametric functions used in the simulation model (red line). The spontaneous dropping rate could not be measured directly; we therefore set it to the linear extrapolation at n = 0, $\eta_{d,0}$ = 0.025 s^{-1}. (*A* and *B*, *Insets*) The corresponding probabilities of depositing and picking up a soil pellet as a function of the number of previously deposited pellets encountered within a radius of 0.5 mm as estimated from experiments. (*C*) Height distribution of pellets deposited along vertical wood pillars (black bars) and the fitted skew normal distribution function (red line). (*C*, *Inset*) The cumulated distribution function $F(h)$ used to modulate the probability of depositing a building particle as a function of the vertical location of ants. (*D*) Test for the presence of pheromone in the material manipulated by ants in a binary choice experiment containing the two types of pillars in the same Petri dish. Dynamics of the fraction of ants around the test pillar made with material recently manipulated by ants (red line ± SE) and the control pillar made with material that has never been in contact with ants (orange line ± SE). The dots indicate the times when the fractions were measured (every 5 min).

those places. However, because the chemical compound evaporates with time, this effect has only a limited duration.

Computational Model. A stochastic, spatially explicit individual-based model (IBM) was developed to understand the respective roles of the individual behavioral rules and the building pheromone in the emergence and characteristics of tridimensional structures built by groups of ants. In the model, the 3D discrete space is defined by a $200 \times 200 \times 200$ cubic lattice with a unit side length $\Delta l = 0.5$ mm. The building material is made of particles whose elementary size corresponds to that of a single cell. Ants are mobile agents, and each of them also occupies a single cell. Because the density of ants remains quite low in the experimental setup, one can consider that there is no cluttering effect that could prevent the workers having access to any potential building site (Movie S1). This condition is in sharp contrast to digging behavior. In that case, the dug galleries and the workers have often the same width, thus limiting an easy access to the digging fronts (34). Hence, although real ants are much larger than the particles of material that they pick up, transport, and deposit, we represented each ant as occupying a single cell in the cubic lattice. One may consider that a cell corresponds to the location of the head of the ant where it performs its building behavior. Each ant can only perceive its 26 neighboring cells in 3D space (hereafter denoted as V_{26}).

In line with previous models of nest building behavior (17, 19), our model also incorporates logistic constraints imposed by the built structures on the motion of ants. Namely, ants move according to a random walk, but they are constrained to stay in contact with the surface of the built structure and cannot walk through cells that are already occupied either by building material or by other ants. Moreover, ants can only move to adjacent locations (i.e., to the six orthogonal locations around the ants' current position). When ants come into contact with the boundaries of the lattice, their motion is randomly reoriented in a direction facing away from these boundaries. The deposition behavior is also conditioned by physical constraints: a building particle can be deposited only at locations where it can share a common face with another particle. Finally, a particle can be deposited in a cell only if there exists an empty adjacent cell where an ant can move after the deposition (see *SI Materials and Methods* for details).

During one time step, agents move as described above, and then they can either (*i*) choose to pick up a particle from the ground if they are not already carrying one with a probability $\widetilde{P}(pick)$, (*ii*) deposit a particle with a probability $\widetilde{P}(drop)$, or (*iii*) simply keep walking. The decision process is local and Markovian: $\widetilde{P}(pick)$ and $\widetilde{P}(drop)$ only depend on the number of particles present in V_{26}. There is no effect of the amount of time an ant has spent either moving unloaded on $\widetilde{P}(pick)$ or carrying a particle on $\widetilde{P}(drop)$. An ant can pick up any particle on the bottom layer of V_{26} and deposit a pellet on the ant's current position, both as a function of previously deposited pellets in V_{26} [$\widetilde{P}(pick) = \widetilde{P}(pick|n)$ and $\widetilde{P}(drop) = \widetilde{P}(drop|n)$]. The model also includes the body-template effect that leads to the lateral depositions of pellets on the sides of pillars that are tall enough. Thus, $\widetilde{P}(drop|n)$ is modulated by the height of the empty space below the current ant's position [simply by multiplying $\widetilde{P}(drop|n)$ by the cumulative density function in the *Inset* of Fig. 3*C*].

Experiments also suggest that ant workers add a pheromone to the building material that may enhance further depositions of pellets at the locations where pheromone intensity is high enough. We have included the chemical marking of building material in the model: once it has been deposited, a particle is labeled by the time of its deposition. As a first approximation, we consider that the diffusion of the pheromone was negligible. We assume that the pheromone decay rate η_m (i.e., the inverse of the mean lifetime of the pheromone) is exponential. Thus, the pheromone provides the ants with local information about the time elapsed since a particle was deposited at a given location. The ants' response to the pheromone is an increase of $\widetilde{P}(drop|n)$ with the total amount of pheromone in the surrounding building material as follows:

$$\widetilde{P}(drop|n, \tau_m) = 1 - e^{\left(-\eta_d(n) \cdot \Delta t \cdot e^{(-\tau_m \cdot \eta_m)}\right)}, \quad [1]$$

where τ_m is the time elapsed since the latest deposition event in V_{26}, and $\eta_d(n)$ is the instantaneous deposition rate (Eq. **S3** in *SI Materials and Methods*). Model simulations were done with a group of 500 ants and updated every $\Delta t = 1$ s.

Estimation of Model Parameters. All parameters of individual ant behaviors were estimated from the experimental data with the exception of the lifetime of the pheromone ($1/\eta_m$), which depends on many parameters such as temperature and humidity (*SI Materials and Methods*). Pheromone lifetime was the only free parameter of the model, and we investigated how it affects the construction dynamics.

Simulation Results and Comparisons with Experimental Data. We investigated the effect of pheromone lifetime on the growth and form of structures built by ants (Fig. 4 *A* and *B* and Fig. S7). Our simulation results show that without the dynamics induced by pheromone marking, no structure can be built (Movie S4). The

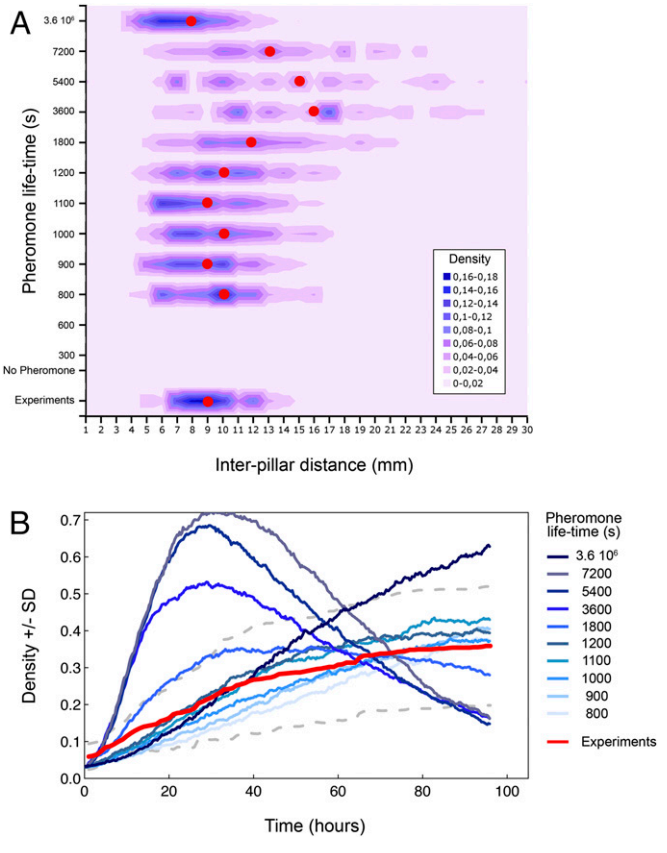

Fig. 4. Effect of the pheromone on the growth and form of built patterns observed in the simulations. (*A*) Distribution of nearest-neighbor distances between pillars after 96 h, measured in the experiments and in the model for different values of pheromone lifetime. The red dots indicate the median of the nearest-neighbor distance between pillars. (*B*) The average density of pillars built as a function of the pheromone lifetime. The red curve indicates the mean of experimental data, and the gray dashed line indicates the SD ($n = 11$). For each value of the pheromone lifetime, 10 numerical simulations were performed with a group of 500 ants.

material that covers the whole surface of the experimental setup is just remodeled, but there is no amplification of depositions at some locations, and as a consequence, no pillar can be built. This result suggests that the pheromone included by ants in the pellets of building material is a key ingredient in the construction process. When the lifetime of the pheromone exceeds 10 min, ants start to build small pillars with an average size that is less than the threshold of 14 mm^2 used to detect pillars in the experiments (Fig. S7 and Movie S5). By chance, the concentration of depositions at some locations creates little heaps that become the seeds from which the ants start to build the pillars; this process results from a positive feedback induced by the pheromone (Fig. 5 *A*–*C* and Movie S6). Then, for higher values of the pheromone lifetime, when pillars become high enough, particles are added on their sides, thus rapidly increasing the surface over which more material can be deposited. The resulting shape of caps built on top of pillars is similar to the shape built by ants in the experiments (Fig. S4*A*). It may also happen that when two neighboring caps are close enough, they can merge, thus forming an arch connecting two pillars (Fig. 5*C*). At a larger scale, the spatial patterns built in the simulations are very close to those observed in the experiments (Fig. 5 *G*–*I*), and a constant remodeling activity of the built structures can also be observed (Movie S7). A closer look at the spatial organization of pellets in the pillars and the visualization of the amount of pheromone present in each pellet also reveals a rich and complex topochemical landscape (Fig. 5 *D*–*F* and Movie S8).

For some values of the pheromone lifetime (800 s $\leq 1/\eta_m \leq$ 1,200 s), the temporal dynamics of the average density of pillars and of the average distance between neighboring pillars, as well as the distribution of distances between neighboring pillars, after 96 h are in close agreement with the temporal and spatial dynamics observed in experiments (Fig. 2 *A*–*E* and Fig. S8). For increasing values of the pheromone lifetime, the median distance between neighboring pillars first increases, reaches a maximum when $1/\eta_m \sim 3{,}600$ s, and then decreases again (Fig. 4*A*). However, one can notice that the corresponding dynamics of the average density of pillars undergoes a drastic change as the pheromone lifetime increases. As construction progresses, the density of built pillars increases until it reaches a maximum for $1/\eta_m \sim 7{,}200$ s, and then it decreases to reach a value comprised between 0.15 and 0.3 pillar/cm^2 (Fig. 4*B*). It can also be observed that the sharpness of dynamics increases with $1/\eta_m$. This particular pattern reflects the merging process of neighboring caps and their lateral growth (Fig. S7 and Movie S9). As a consequence, the total number of distinct structures built above 3 mm (the criterion that was used for counting pillars) diminishes (Fig. 4*B* and Fig. S8). Such dynamics are somewhat quite different from those observed in the experiments, because in the latter, the average density reaches a plateau around 72 h. Moreover, even if some merging events are observed in experiments, the enlargement and the flattening of caps over the pillars is not as important as the merging events observed for larger values of $1/\eta_m$. We have finally investigated a situation in which the lifetime of the pheromone was much larger than the total duration of simulations (Fig. 4 *A* and *B*, Movie S10, and Fig. S8). In that case, we found a very large number of small pillars with an average distance between neighboring pillars of ∼8 mm. Over the long term, the whole building material becomes saturated with pheromone and the pellets are evenly deposited. The first pillars are then progressively eroded because of the remodeling process, but no other built structure can emerge anymore. All combined, these results suggest that a reasonable value for the pheromone lifetime in our experimental conditions would be between 800 and 1,200 s.

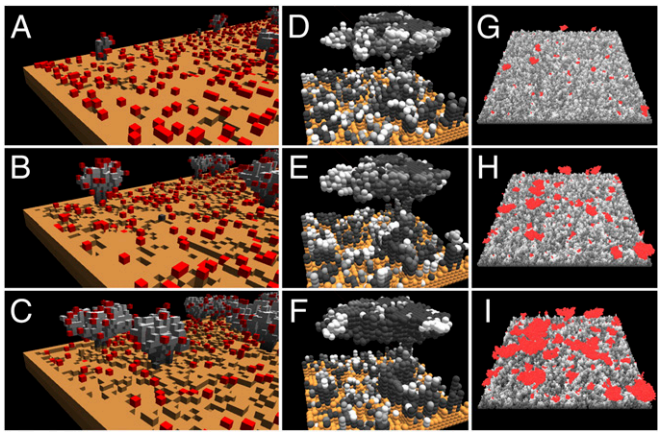

Fig. 5. Three-dimensional simulations of ant nest construction. (*A*–*C*) Sequence that shows the emergence of two pillars that are joined by an arch (ants are the red cells, brown cells are the initial construction material, and gray cells are moved pellets/cells). (*D*–*F*) Three simulation runs of a pillar construction showing the complex topochemical landscape created by the heterogeneous amount of pheromone in the building pellets (the gray scale indicates the amount of pheromone, the most recently deposited pellets are in light gray, and the oldest pellets are in dark gray). (*G*–*I*) The same representation on a larger scale, with emerging structures above a height of 3 mm colored in red (*G*, after 24 h; *H*, after 48 h; *I*, after 96 h). All simulations were run with a pheromone mean lifetime of $1/\eta_m$ = 20 min and 500 ants.

Discussion

Nest construction by social insects is a classic example of biological morphogenesis (35, 36). Therefore, identifying the underlying mechanisms involved in the coordination of building behavior is of fundamental importance to understand the growth and form of nest architecture. Here, we have characterized the individual behaviors involved in nest building in the ant *L. niger*, and we have constructed a 3D model for disentangling the coordinating mechanisms at work. This is the first study to our knowledge that addresses 3D nest morphogenesis in social insects through a tight coupling of experiments and data-driven modeling. Our results indicate that the coordination of building actions was achieved through two main interactions: (*i*) a stigmergic-based interaction that controls the amplification of depositions at some locations and the emergence of pillars and is attributable to a pheromone added by ants to the building material; and (*ii*) a template-based interaction between the ant's body and the growing structures that controls the height at which ants start to build a roof from an existing pillar. The model shows that this simple set of interactions and building rules can reproduce the key features of construction dynamics that have been observed experimentally in the ant *L. niger*, including a large-scale pattern of regularly spaced pillars, the formation of caps over the pillars and their subsequent merging, and the remodeling of the built structures. A similar combination of mechanisms involving self-organization and template has been described in the construction and size regulation of the encircling wall in the ant *Leptothorax tuberointerruptus*, which builds simple bidimensional nests within flat crevices (27). This finding suggests that common coordination mechanisms might govern the growth and adaptation of nest architecture in ant colonies. In *L. niger*, the combination of information provided by the material patterns and the local concentration of pheromone extends the richness of stimuli used by ant workers to guide their building activity. Thus, depending on the amount of chemical signal impregnating the surface of a built structure, the same 3D constructed pattern can elicit different building responses from the ants. Moreover, the heterogeneous spatial distribution of the pheromone present on the built surface creates a topochemical landscape that determines the rate of deposition of new pellets.

The pheromone thus controls the local growth dynamics and the resulting nest architecture.

With the exception of the pheromone lifetime ($1/\eta_m$), all behavioral parameters have been quantified in dedicated experiments, and the model's predictions have been confronted with measurements on the structures built by ants in the field and in the controlled experiments. A sensitivity analysis was used to determine the value of $1/\eta_m$ (between 800 and 1,200 s), leading to construction dynamics and spatial patterns similar to those observed in the experiments. This estimated value of the pheromone lifetime is of the same order as that of the trail pheromones described in many ant species [e.g., about 10 min in *Monomorium pharaonis* (37), 10–20 min in *Solenopsis saevissima* (38), and up to 30 min in *Linepithema humile* (39)].

The model was then used to assess the role of the pheromone on building activity. The simulation results clearly indicate that the pheromone is an essential ingredient to induce a positive feedback and ensure the growth of the basic elements from which the ant nest is made. In absence of pheromonal marking, ants would not be able to distinguish marked from unmarked building material. Moreover, the lifetime of the pheromone governs the characteristic spacing between adjacent pillars. Hence, because temperature and humidity strongly influence the pheromone's mean lifetime, the pheromone is likely to play a key role in the phenotypic plasticity of nest architecture in *L. niger*. The pheromone directly modulates the local behavioral response of ants to the previously built structures without having a direct impact on the flows of ants carrying building material. This mechanism is in sharp contrast to previous hypotheses introduced by Deneubourg (40) in a simple 1D construction model. In this model, the emergence of regularly spaced pillars was resulting from a pheromone-driven advection of insects with no interaction between them and the building material (i.e., the picking-up and deposition rates are constant). Our results show that in *L. niger*, construction behavior is based on a direct and local interaction between the individuals and the material used to build the nest, needing no more than a simple diffusive movement of ants constrained by the evolving and collectively built surface over which they move.

One can finally notice that the structural stability of the nests built by ants requires a minimal density of pillars, so that caps can easily merge, form arches between neighboring pillars, and endure desiccation. A regular spacing of pillars also favors a uniform growth of the roof. Remarkably, the typical interdistance between pillars is robustly driven by the behavioral parameters and the pheromone lifetime; neither the number of ants (Fig. S9) nor the available space (Fig. S10) affects the spacing between pillars. In biological systems, processes based on a local-activation and long-range inhibition (41) provide a simple and efficient way to get such regular patterns, and the existence of these processes has been demonstrated to govern the spatial organization of corpse aggregates in the ant *Messor sancta* (28). In *L. niger*, pillar formation is based on a similar logic. However, positive and negative feedbacks that support self-organization are implemented in different ways. Whereas in *M. sancta*, negative feedback mainly results from the depletion of corpses from which clusters are made, in *L. niger*, the negative feedback simply results from the evaporation of the pheromone. Thus, simple behavioral rules whose execution depends on local cues (density of marked material and body size) ensure an economic coding of the processes required for building a complex 3D nest structure by a group of insects. In this way, similar individual rules can be involved in many different collective behaviors, from corpse aggregation to nest building.

ACKNOWLEDGMENTS. We thank Noa Pinter-Wollman for useful comments and suggestions on the manuscript. We are grateful to Richard Fournier and Stéphane Blanco (Laboratory on Plasma and Conversion of Energy, Université Toulouse III) for providing us the computer facilities that were essential for this work. We also thank Nathalie Boulic, Marion Keromest, Julie Olivera, Victor Loisel, Mathieu Moreau, and Théo Robert for research and technical assistance. This work was supported by ANR-06-BYOS-0008. A.K. was supported by a doctoral grant from the PRES University of Toulouse/Région Midi-Pyrénées (APR 2010).

1. Wilson EO (1971) *The Insect Societies* (Harvard Univ Press, Cambridge, MA).
2. Tschinkel WR (2004) The nest architecture of the Florida harvester ant, *Pogonomyrmex badius*. *J Insect Sci* 4:21.
3. Hansell M (2005) *Animal Architecture* (Oxford Univ Press, New York).
4. Tschinkel WR (2005) The nest architecture of the ant, *Camponotus socius*. *J Insect Sci* 5:9.
5. Grassé PP (1984) *Termitologia, Tome II* (Fondation des Sociétés–Construction, Masson, Paris).
6. Wenzel JW (1991) Evolution of nest architecture. *The Social Biology of Wasps*, eds Ross KG, Matthews RW (Cornell Univ Press, Ithaca, NY), pp 480–519.
7. Turner JS (2000) *The Extended Organism. The Physiology of Animal-Built Structures* (Harvard Univ Press, Cambridge, MA).
8. Kleineidam C, Roces F (2000) Carbon dioxide concentrations and nest ventilation in nests of the leaf-cutting ant *Atta vollenweideri*. *Insectes Soc* 47(3):241–248.
9. Korb J (2003) Thermoregulation and ventilation of termite mounds. *Naturwissenschaften* 90(5):212–219.
10. King H, Ocko S, Mahadevan L (2015) Termite mounds harness diurnal temperature oscillations for ventilation. *Proc Natl Acad Sci USA* 112(37):11589–11593.
11. Perna A, et al. (2008) The structure of gallery networks in the nests of termite Cubitermes spp. revealed by X-ray tomography. *Naturwissenschaften* 95(9):877–884.
12. Perna A, et al. (2008) Topological efficiency in three-dimensional gallery networks of termite nests. *Physica A* 387(24):6235–6244.
13. Korb J, Linsenmair E (1999) The architecture of termite mounds: A result of a trade-off between thermoregulation and gas exchange? *Behav Ecol* 10(3):312–316.
14. Bollazzi M, Roces F (2007) To build or not to build: Circulating dry air organizes collective building for climate control in the leaf-cutting ant *Acromyrmex ambiguous*. *Anim Behav* 74(5):1349–1355.
15. Grassé PP (1959) La reconstruction du nid et les coordinations inter-individuelles chez *Bellicositermes Natalensis* et *Cubitermes* sp. La théorie de la stigmergie: Essai d'interprétation du comportement des termites constructeurs. *Insectes Soc* 6(1):41–81.
16. Theraulaz G, Bonabeau E (1999) A brief history of stigmergy. *Artif Life* 5(2):97–116.
17. Theraulaz G, Bonabeau E (1995) Coordination in distributed building. *Science* 269(5224):686–688.
18. Bonabeau E, et al. (1998) A model for the emergence of pillars, walls and royal chambers in termite nests. *Philos Trans R Soc London B Biol Sci* 353(1375):1561–1576.
19. Ladley D, Bullock S (2005) The role of logistic constraints in termite construction of chambers and tunnels. *J Theor Biol* 234(4):551–564.
20. Sudd JH (1970) The response of isolated digging worker ants *Formica lemani* Bondroit and *Lasius niger* (L.) to tunnels. *Insectes Soc* 49(4):261–272.
21. Sudd JH (1971) The effect of tunnel depth and of working in pairs on the speed of excavation in ants (*Formica lemani* Bondroit). *Anim Behav* 19(4):677–686.
22. Rasse P, Deneubourg JL (2001) Dynamics of nest excavation and nest size regulation of *Lasius niger* (Hymenoptera: Formicidae). *J Insect Behav* 14(4):433–449.
23. Mikheyev AS, Tschinkel WR (2004) Nest architecture of the ant *Formica pallidefulva*: Structure, costs and rules of excavation. *Insectes Soc* 51(1):30–36.
24. Buhl J, Deneubourg JL, Grimal A, Theraulaz G (2005) Self-organized digging activity in ant colonies. *Behav Ecol Sociobiol* 58(1):9–17.
25. Toffin E, Di Paolo D, Campo A, Detrain C, Deneubourg JL (2009) Shape transition during nest digging in ants. *Proc Natl Acad Sci USA* 106(44):18616–18620.
26. Franks NR, Wilby A, Silverman BW, Tofts C (1992) Self-organizing nest construction in ants: Sophisticated building by blind bulldozing. *Anim Behav* 44(2):357–375.
27. Franks NR, Deneubourg Jl (1997) Self-organizing nest construction in ants: Individual worker behaviour and the nest's dynamics. *Anim Behav* 54(4):779–796.
28. Theraulaz G, et al. (2002) Spatial patterns in ant colonies. *Proc Natl Acad Sci USA* 99(15):9645–9649.
29. Sudd JH (1967) *An Introduction to The Behaviour of Ants* (Edward Arnold, London).
30. Howse PE (1970) *Termites: A Study in Social Behaviour* (Hutchinson, London).
31. Bruinsma OH (1979) An analysis of building behaviour of the termite *Macrotemes subhyalinus*, PhD thesis (Lanbouwhogeschoolte, Wageningen, The Netherlands).
32. Jones RJ (1979) Expansion of the nest in Nasutitermes costalis. *Insectes Soc* 26(4):322–342.
33. Petersen K, et al. (2015) Arrestant property of recently manipulated soil on *Macrotermes michaelseni* as determined through visual tracking and automatic labeling of individual termite behaviors. *Behav Processes* 116:8–11.
34. Monaenkova D, et al. (2015) Behavioral and mechanical determinants of collective subsurface nest excavation. *J Exp Biol* 218(Pt 9):1295–1305.
35. Murray JD (1993) *Mathematical Biology* (Springer, Heidelberg), 2nd Ed.
36. Ball P (2011) *Shapes: Nature's Patterns: A Tapestry in Three Parts* (Oxford Univ Press, New York).
37. Jeanson R, Ratnieks FLW, Deneubourg J-L (2003) Pheromone trail decay rates on different substrates in the Pharaoh's ant, *Monomorium pharaonis*. *Physiol Entomol* 28(3):192–198.
38. Wilson EO (1962) Chemical communication among workers of the fire ant *Solenopsis saevissima* (Fr. Smith) 1. The organization of mass-foraging. *Anim Behav* 10(1-2):134–147.
39. Perna A, et al. (2012) Individual rules for trail pattern formation in Argentine ants (*Linepithema humile*). *PLOS Comput Biol* 8(7):e1002592.
40. Deneubourg JL (1977) Application de l'ordre par fluctuation à la description de certaines étapes de la construction du nid chez les termites. *Insectes Soc* 24(2):117–130.
41. Meinhardt H (1982) *Models of Biological Pattern Formation* (Academic, London).
42. Bhaktar AP, Whitcomb WH (1970) Artificial diet for rearing various species of ants. *Fla Entomol* 53:229–232.

Supporting Information

Khuong et al. 10.1073/pnas.1509829113

SI Materials and Methods

Study Species. Experiments were carried out with colonies of the ant *L. niger*, a common monogynous and monomorphic Palearctic species whose colony size may vary from thousands to tens of thousands of individuals. Thirteen colonies were collected between 2006 and 2010, either on the Campus of the Paul Sabatier University in Toulouse, France (43°33′35.24″ N, 1°28′25.74″ E), or in the countryside near Ramonville, France (43°32′37.07″ N; 1°29′38.27″ E), and Marquefave, France (43°19′12.57″ N; 1°14′52.26″ E). The colonies were reared in the laboratory under controlled temperature (25 ± 2 °C), humidity level (30–40%), and photoperiod (12-h light:12-h dark) conditions. Each colony containing about 2,000–3,000 workers (with brood but no queen) was housed in a plastic box of 100 mm diameter (nest-box) placed inside a square foraging box of size 270 mm × 270 mm. The walls of the boxes were coated with Fluon to prevent ants from escaping. Ants were fed three times a week with a mixed diet of vitamin-enriched food [modified after Bhaktar and Whitcomb (42)] and maggots.

Whole Nest Acquisition with X-Ray CT. Two *L. niger* mounds built in natural conditions from meadows were collected near Marquefave, France. Mound A (Fig. 1*A*) measured 27 cm (height) with a diameter of 26 cm, whereas mound B measured 21 cm (height) with a diameter of 27 cm. The mounds were imaged with X-ray CT (Somatom Sensation 16 scanner) and reconstructed into stacks of digital images with pixel resolutions of 0.53 and 0.69 mm for mound A and B, respectively, a slice thickness of 1 mm, and an interslice distance of 0.5 mm.

Analysis of Tomographic Images of the Nests. The nest walls were segmented from the background by applying an iterative self-organizing data analysis technique (IsoData) threshold algorithm independently on each slice. To further separate the galleries internal to the nest from the outside air, we created a mask that had roughly the same shape as the nest and applied the mask to classify the voxels that represent empty space as either internal galleries or outside air. The mask was simply obtained through an operation analogous to a 3D morphological closing of the nest walls. More precisely, the nest walls were first dilated by convolving them with balls of radius 10 voxels. This operation removed the galleries internal to the nest (whose radius was typically smaller than the radius of the structuring balls) and also part of the outside air in the immediate proximity of the nest. To further eliminate any possible leftover empty space inside the nest, we further selected only the largest connected component of empty space, corresponding to the outside air. Finally, the identified connected component of outside space was dilated through the convolution with structuring balls of 14 voxels radius, to obtain the final mask.

After applying the mask to the initial thresholded images, we obtained 3D volumes in which all of the empty space internal to the nest was labeled as internal galleries. This empty space comprised the galleries used as a nest by ants but occasionally also older, partially collapsed sections of galleries that were no longer connected to the main nest as well as a small number of grass straws (these latter are easily recognizable in the images because of their small diameter and straight continuity). We excluded the grass straws by applying a morphological closing operation to the internal galleries, comprising erosion of one single voxel followed by dilation of one voxel). The erosion operation was sufficient to relabel the thin galleries produced by straws as nest walls, and the dilation operation restored the original size of real ant galleries. We also excluded old, isolated and collapsed chambers by focusing all subsequent analysis only on the largest connected component of the internal gallery system. From the internal galleries identified above, we computed a 3D digital skeleton by applying a 3D morphological skeletonization algorithm (plugin skeletonize3D in ImageJ).

Measuring the Height and Width of Chambers and Galleries from Tomographic Data. The nests obtained from the field do not present an immediately recognizable organization in pillars and layers: some pillars appear to have been connected to form walls (something that was occasionally also observed in the laboratory experiments), and layers are not perfectly horizontal. These differences could possibly result from collapses and rebuilding of individual nest sections. For these reasons, we could not calculate directly the minimum distance between nearest-neighbor pillars and the height of pellet deposition around a pillar, and we preferred to focus on the following two measures of vertical and horizontal spacing between nest elements: gallery height and minimum horizontal gallery width.

The height of galleries was estimated in correspondence to each voxel of the digital skeleton by measuring the vertical height of the gallery above and below the skeleton point. This measure is expected to provide an approximation of the minimum height of pellet deposition on a pillar. The approximation is also expected to be by excess, first because the skeleton runs through the central part of each gallery and not in the adjacency of a pillar, where the ceiling is likely lower, and second because the layers are not perfectly horizontal.

The width of galleries was also estimated in correspondence to each voxel of the digital skeleton by measuring the horizontal distance to the center of the nearest wall and multiplying it by two (because the skeleton runs through the center of the gallery with good approximation its minimal distance to the nearest wall is similar to the minimal distance to the opposite wall). This measure is expected to provide an approximation of the nearest-neighbor interpillar distance.

Experimental Setup Used for Quantifying Collective Construction Dynamics and Spatial Patterns. The experimental setup consisted of a 10 cm diameter Petri dish with a sidewall height of 1cm, which was stuck to the top of a 5 cm high circular plastic box filled with water. The two modules were connected by a cotton wick that led from the water-filled bottom box through the floor of the upper part. The Petri dish was first covered with a thin layer of plaster embedding the cotton wick (about 8 mm high), which allowed the water to infiltrate and percolate. The plaster layer was then covered with a thin layer of sand–clay mixture in equal proportion (10 g dry weight). The water diffused from the plaster and maintained a high level of moisture in the building material. The layer of moistened building material, about 2–3 mm high, was not high enough for allowing the ants to dig tunnels. The set up was placed within a larger plastic container (27 cm × 27 cm), the walls of which were coated with Fluon to prevent the ants from escaping. The container was provided with a water-filled plastic tube capped with cotton and food (protein/sugar) supplies. Groups of 500 ants randomly selected from their colonies were then introduced into the container, and their building activity was recorded for a whole week. The setup was lit twenty-four hours a day, thus creating a condition that strongly stimulated the building activity of ants (to produce shaded shelters). Temperature and relative humidity (RH) were kept constant (26 °C and 30 – 40% RH, respectively). The experiment was replicated 11 times.

To quantify the structures built by ants, we used a NextEngine 3D Laser scanner (www.nextengine.com). The scanner was mounted vertically above the Petri dish (Fig. S3 *A* and *B*) and was controlled by a remote computer and the software Scan Studio 1.3.0 and xStarter 1.8.8. The acquisition frequency was set to one scan per hour. This tool produced a time series of detailed height maps of the soil surface in the Petri dish with a spatial resolution of 150 μm. Thus, it was possible to locate the initiation and the growth of pillars, up to the construction of lateral extensions when pillars were tall enough. The surface scan data were first preprocessed to get a time series of matrices (400×400) with a spatial resolution of 0.3 mm and an average height of the initial sand–clay surface of 0 mm (Movie S2). The height map was then binarized at a height of 3 mm, so that each growing pillar can be easily identified once it has reached a minimum surface area of 14 mm^2 and then tracked all along the sequence of surface scans. From these data, we got the total number of pillars built by ants and the distance of each pillar to its nearest neighbor. Because some variability was observed across experiments regarding the initiation of the ants' building activity, we considered a situation when at least three pillars were built as the start time of each experiment. Then, the experimental data were properly aligned in time against their respective start time and averaged. The resulting time series were finally smoothed by a moving average over a 2-h time window.

Experimental Setup Used to Quantify the Modulation of the Picking Up and Deposition Behaviors by the Previously Built Structures. To analyze the picking-up and dropping behaviors, we used a 6-cm-diameter Petri dish stuck onto a 3.5-cm-high circular plastic box filled with water (Fig. S5 and Movie S3). The two modules were connected by a cotton wick that led from the water-filled bottom box through the floor of the upper part. The central part of the Petri dish was covered with a 4-cm-diameter circular layer of plaster embedding the cotton wick (about 2 mm high), which allowed the water to infiltrate and percolate. The Petri dish is then covered with a red color filter glass to block out visible light. Ants can get access to the Petri dish through a 5-mm circular hole cut in the sidewall. The setup was placed within a larger plastic container ($27\ cm \times 27\ cm$), the walls of which were coated with Fluon to prevent the ants from escaping. The container was provided with a water-filled plastic tube capped with cotton and food (protein/sugar) supplies. A group of 750 ants randomly selected from their colonies was then introduced into the container, for a period of 1 wk, in order for the ants to settle into the Petri dish. At the beginning of the experiment, the red color filter glass is removed and two small dishes filled with wet clay are set down on a cardboard platform next to the entrance hole. Clay is rapidly collected by ants, transported in the Petri dish and used by ants as building material. The clay is kept humidified during the whole experiment, and the dishes are changed every day. The behavior of ants in the Petri dish is recorded from above using a video camera (Sony CCD-IRIS; 18–108 mm) for 8 h. Temperature and RH were kept constant (26 °C and $30-40\%$ RH, respectively). The experiment was replicated six times.

Experimental Setup Used to Quantify the Vertical Modulation of Deposition Behavior by the Previously Built Structures. In these experiments we used the ants' tendency to deposit preferentially on vertical surfaces. The experimental setup was the same as that for the collective construction experiments detailed above, covered with 15-g sand–clay mixture and containing four aligned and equally spaced vertical wood sticks of diameter 2 mm and extending 1.5 cm beyond the sand–clay mixture. Each of the 4 replications used 500 ants and lasted 48 h. At the end we measured on each wood stick the minimal and maximal height of construction and the height with the highest horizontal extension. Construction activity was highly variable across wood sticks, the measured height sometimes concerning a single soil pellet. We therefore used these heights as simple soil presence indicators and assembled them to construct the density distribution along the vertical surface (Fig. 3*C*).

Experimental Setup Used to Test the Presence of Pheromone in the Building Material. To test the presence of a pheromone included by the ant workers in the pellets of building material, we used nearly the same setup as in the collective construction experiments. The plaster was divided into two zones: a 2-cm-wide and 5-mm-deep annular area adjacent to the outer border and filled with the sand–clay mixture and a central 6-cm-diameter disk of bare plaster level with the Petri dish border. On this disk, we placed two hand-formed pillars with ∼1 cm diameter, 2 cm height, and 3 cm distance from each other: one made of new sand–clay mixture and one made with the mixture that had just been processed by the ants in a parallel ongoing construction experiment. Immediately after forming this pillars, we added 500 ants and filmed the setup for 0.5 s every 5 min from the top during 10 h (Sony DCR VX 1000E). Eight replications of this experiment were run. The ants typically gathered around one pillar. We assessed which pillar was first chosen, and we counted every 5 min the number of ants within a 2-cm-diameter circle centered on each pillar.

Estimation of the Picking-Up Probabilities. To determine the probability $P(pick|n)$ that an ant picks up a pellet on a pile of n previously deposited pellets, we focused on six different sites where the largest piles emerged at the end of the observation ($T = 4$ h). We played the videotape backward and recorded all of the contacts that ants had with those six piles, whether they were carrying a pellet or not, as well as all of the depositions and picking-up events on the piles, until the very first depositions. Let μ_c be the contact rate between ants carrying a pellet and a pile and μ_u be the contact rate of unloaded ants with a pile. The total rate of contacts $\mu = \mu_c + \mu_u$ can be estimated by the distribution of times between two contacts with a pile. We can fit the survival time between two consecutive contacts with a pile to a Weibull function (for example, see www.mathpages.com/home/kmath122/kmath122.htm): $W(t) = e^{-(\mu \cdot t)^{\alpha}}$. We found $\alpha \simeq 1.0$, meaning that the survival time followed an exponential decay, with $\mu = 0.22 \pm 0.005\ s^{-1}$. We then determined the probability that an ant contacting a pile was carrying a pellet and found that $P_{carrying} = 0.32 \pm 0.02$, from which we got an estimation of $\mu_c = \mu \cdot P_{carrying} = 0.0704\ s^{-1}$ and $\mu_u = \mu \cdot (1 - P_{carrying}) = 0.1496\ s^{-1}$. From the depositions and picking-up events, we were also able to estimate the rate of change $\nu(n)$ of a pile of size n, either by increasing or decreasing the number of the pile's constituent pellets. Thus, $\nu(n) = \mu_c \cdot P(drop|n) + \mu_u \cdot P(pick|n)$. Let $P(increase|n)$ be the probability that a pile of size n increases its size when pile size changes. From the estimation of $P(increase|n)$ for each pile of size n (the ratio of the number of increasing changes to the total number of changes), we were able to determine the corresponding values of $P(pick|n)$. We have: $\mu_c \cdot P(drop|n) = \nu(n) \cdot P(increase|n)$, meaning that the rate of increasing size change of a pile equals the deposition rate of pellets by ants. We then have

$$\nu(n) = \nu(n) \cdot P(increase|n) + \mu_u \cdot P(pick|n), \qquad [S1]$$

thus

$$P(pick|n) = \frac{\nu(n) \cdot (1 - P(increase|n))}{\mu_u}. \qquad [S2]$$

Estimation of Model Parameters. We used the instantaneous individual rates of picking up $\eta_p(n)$ and depositing $\eta_d(n)$ a particle on a pile of n previously deposited particles to calibrate the probabilities $\tilde{P}(pick)$ and $\tilde{P}(drop)$ in the model. $\eta_p(n)$ and $\eta_d(n)$ are

expressed in s^{-1} and have to be considered as the intrinsic measures of the stochastic decisions performed by ants. These rates are independent of the contact duration of an ant with a pile or the time step used in the model. For a contact lasting Δc seconds, the probability $P(drop|n)$ estimated from the experiments depends on $\eta_d(d)$ as follows:

$$P(drop|n) = 1 - e^{(-\eta_d(n)\cdot\Delta c)}. \quad \text{[S3]}$$

$\eta_d(n)$ can therefore be computed from the experimentally measured $P(drop|n)$ as follows:

$$\eta_d(n) = -\log(1 - P(drop|n))/\Delta c \quad \text{[S4]}$$

(Fig. 3; $\Delta c = 1$ s). The same procedure is used for determining $\eta_p(n)$ from $P(pick|n)$. We then obtained the picking-up and deposition rates for each pile of size n (Fig. 3 *A* and *B*, solid dots). The dependence of deposition and picking-up rates on the number of previously deposited particles n can be modeled as $\eta_d(n) = \eta_{d,0} + b_d\, n$ and $\eta_p(n) = \frac{\eta_{p,1}}{n}$. Parameters were estimated by a linear or nonlinear least-squares method. We found $\hat{\eta}_{d,0} = 0.025$ s^{-1} (used as an estimation of the spontaneous deposition rate), $\hat{b}_d = 0.11$ s^{-1} $pellet^{-1}$, and $\hat{\eta}_{p,1} = 0.029$ s^{-1} (Fig. 3 *A* and *B*, red lines).

To calibrate the vertical modulation of $\widetilde{P}(drop)$, we used the experimental distribution of depositions heights on the wood pillars. Let $f(h)$ be the probability density function for an ant to fasten a building particle on the vertical surface, provided that it reaches the height h still carrying a particle. A skew normal distribution was used to fit the observed data:

$$f(h) = \frac{1}{\omega\pi} e^{-\frac{(h-\xi)^2}{2\omega^2}} \int_{-\infty}^{\alpha\left(\frac{h-\xi}{\omega}\right)} e^{-\frac{t^2}{2}} dt, \quad \text{[S5]}$$

where $\xi = 2.866$, $\omega = 3.727$, and $\alpha = 8.582$ are, respectively, the location, scale, and shape parameters (Fig. 3*C*). However, all locations are not equally sampled by ants, because in most cases, ants have to move over the pillars from the bottom. This constraint reduces the flux of ants carrying particles that can actually reach the highest locations. In the model, to take into account this censoring effect of the highest locations, the probability of depositing a building particle on a vertical location was expressed in the following way:

$$\widetilde{P}(drop|n,h) = \widetilde{P}(drop|n)\cdot F(h), \quad \text{[S6]}$$

where $F(h)$ corresponds to the cumulative distribution function of $f(h)$ (Fig. 3*C*, *Inset*).

The diffusion motion of ants was implemented by allowing them to perform a fixed number of discrete spatial moves per time step (m), so as to reproduce the observed diffusion coefficient of ants walking on a flat surface. We performed simulations of ants with different values of m, we computed for each of them the mean square displacement, $\Delta l^2 \cdot \Delta t^{-1}$, and we determined the value of m that best fit the corresponding experimental data. We found that $m = 1{,}500$ elementary moves by Δt were needed to fit with the biological mean square displacement (87 $mm^2 \cdot s^{-1} = 348$ $\Delta l^2 \cdot \Delta t^{-1}$ with $\Delta l = 0.5$ mm and $\Delta t = 1$ s).

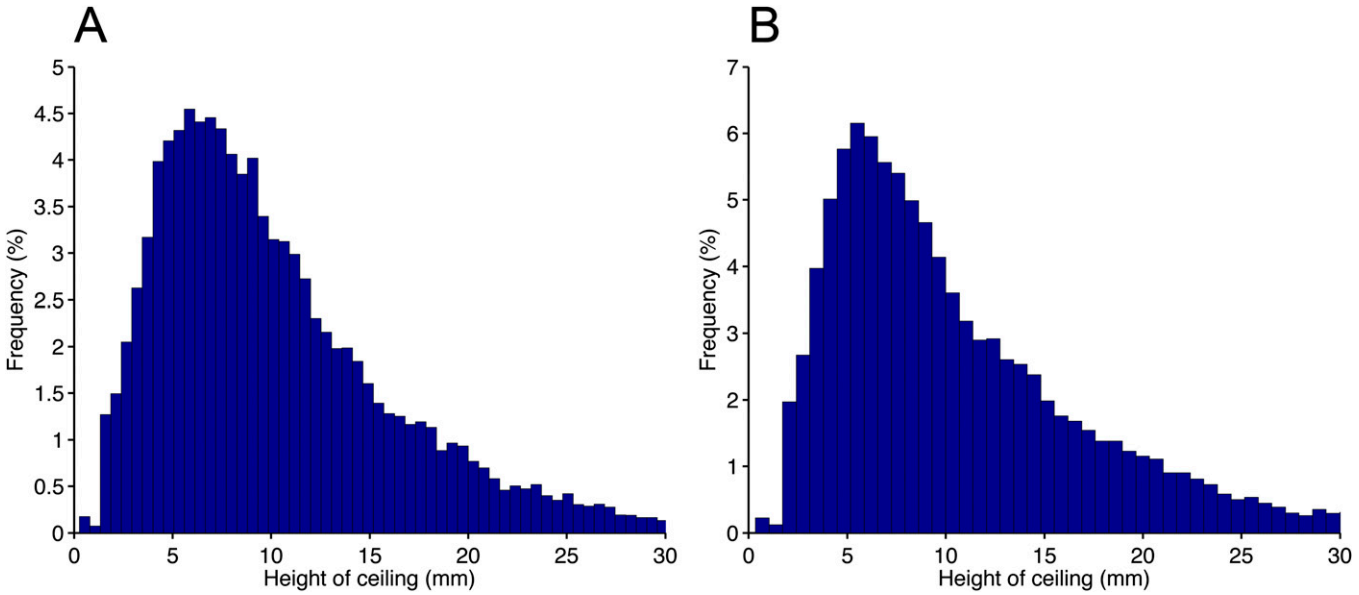

Fig. S1. Distribution of height of all of the chambers and galleries in *L. niger* nests A (*A*) and B (*B*).

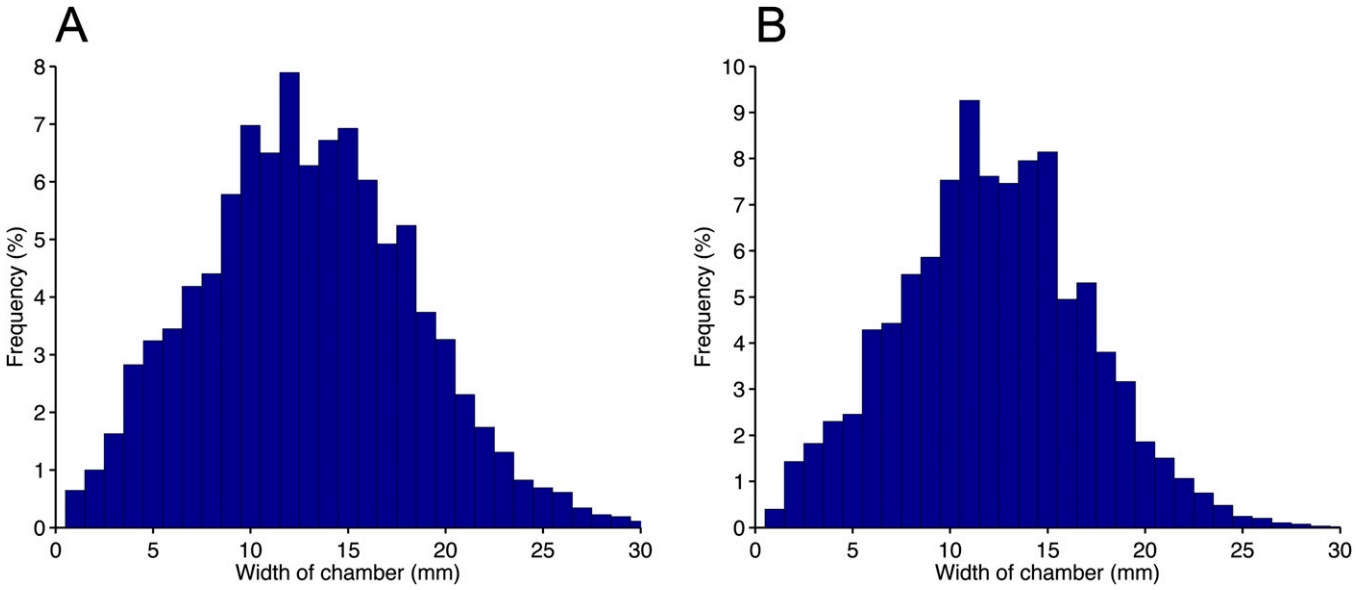

Fig. S2. Distribution of the chambers and galleries widths in *L. niger* nests (*A*) and B (*B*).

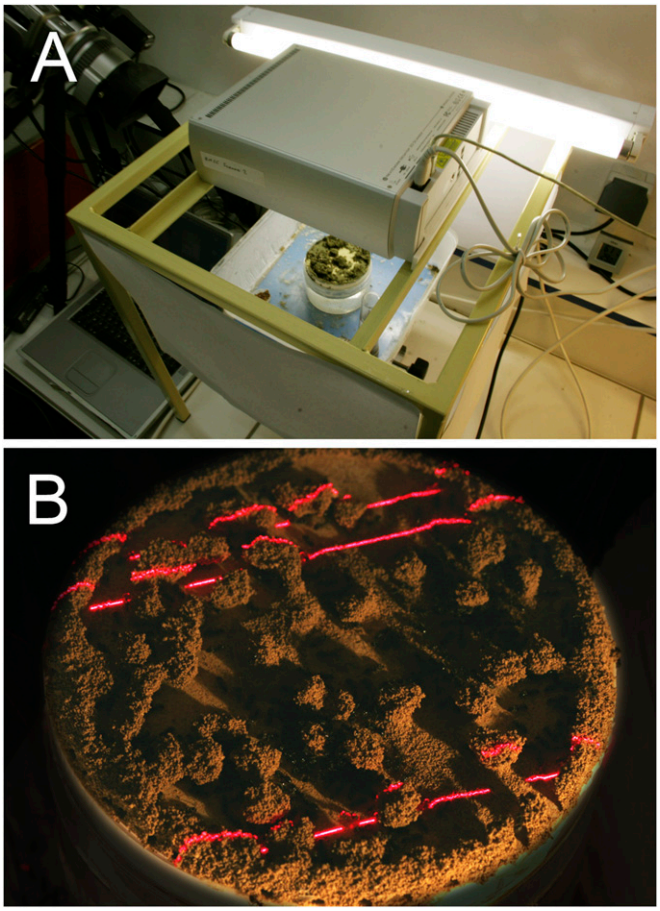

Fig. S3. Experimental set-up used to quantify the construction dynamics and the resulting structures built by ants. A surface scanner is held over the setup (*A*) and is used to record at regular time intervals a 3D image of the spatial pattern resulting from the building activity of ants (*B*).

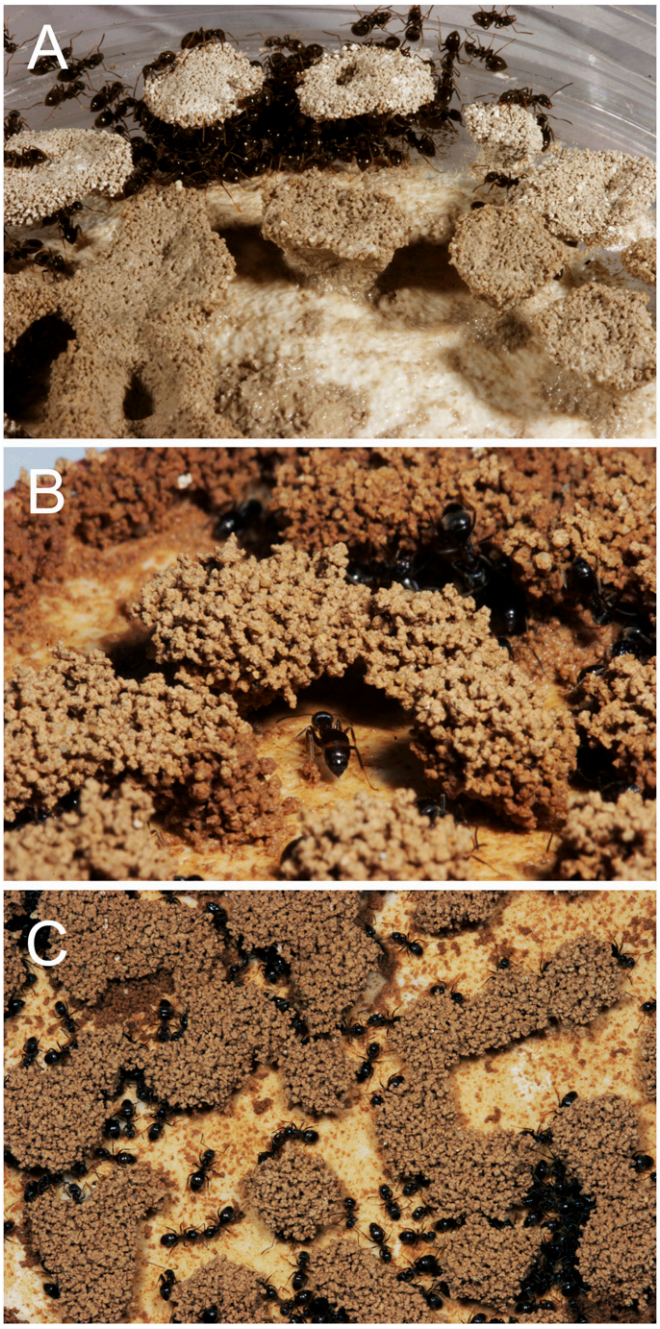

Fig. S4. A few examples of the structures built by groups of 500 ants in experiments. (*A*) The basic elements are pillars whose diameter widens with height. (*B*) The extension of the caps' surface over the pillars may lead two nearby caps to merge and form an arch that covers passages between pillars. (*C*) Groups of neighboring pillars can be connected in the same way, progressively increasing the covered surface.

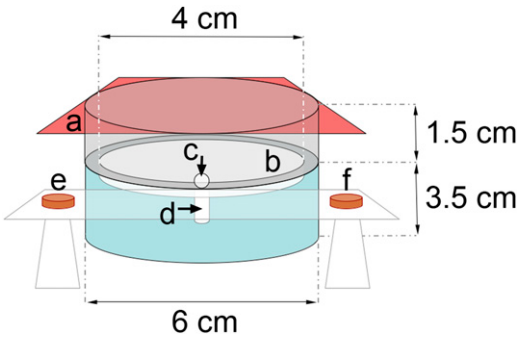

Fig. S5. Schematic diagram of the experimental setup used to quantify the picking-up and deposition behaviors by individual ants: a, red color filter glass; b, circular layer of plaster; c, entrance of the Petri dish; d, cotton wick; e and f, small dishes filled with wet clay.

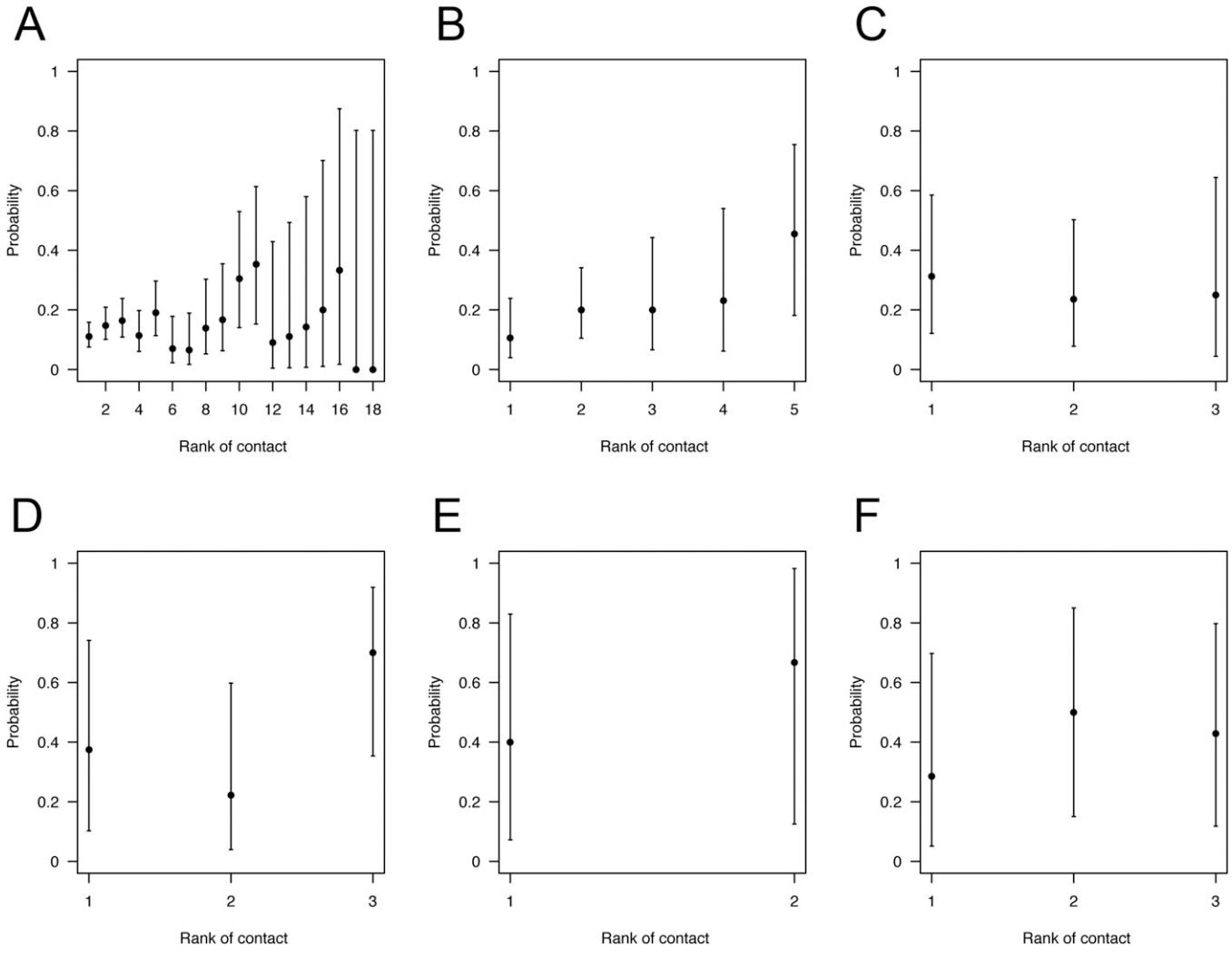

Fig. S6. Influence of the previous contacts of ants with piles on the probability to deposit a pellet. For each size of the pile, we estimated $P(drop|n, r)$ the probability to deposit a pellet as a function of the rank of the events (contact or deposition) from the video sequences. *A–F* correspond to the probability to deposit a pellet (solid dots) as a function of the rank for different sizes of piles. (*A*) One previously deposited pellet. (*B*) Pile of two previously deposited pellets. (*C*) Pile of three previously deposited pellets. (*D*) Pile of four previously deposited pellets. (*E*) Pile of five previously deposited pellets. (*F*) Pile of six previously deposited pellets.

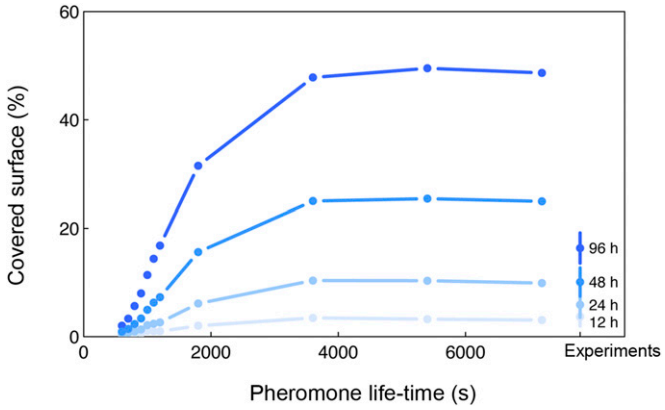

Fig. S7. The average fraction of surface built above 3 mm over the pillars as a function of the pheromone lifetime after 12, 24, 48, and 96 h and the corresponding values measured in the experiments ($n = 11$). For each value of the pheromone lifetime, 10 numerical simulations were performed with a group of 500 ants.

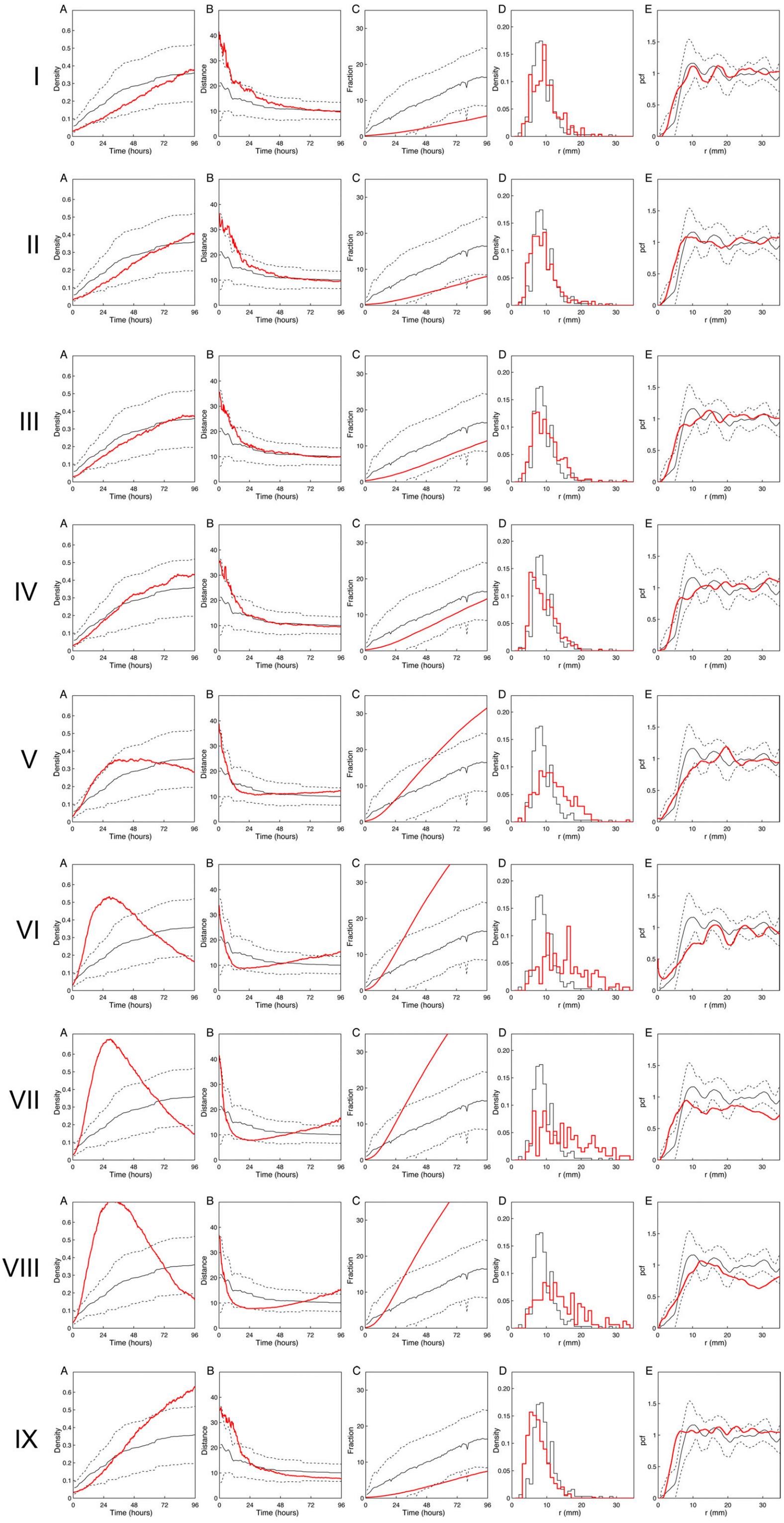

Fig. S8. Construction dynamics and spatial patterns: comparison between the observed data and simulated data with a group of 500 ants and $\frac{1}{\eta_m}$ = 800 s (row I), $\frac{1}{\eta_m}$ = 900 s (row II), $\frac{1}{\eta_m}$ = 1,000 s (row III), $\frac{1}{\eta_m}$ = 1,100 s (row IV), $\frac{1}{\eta_m}$ = 1,800 s (row V), $\frac{1}{\eta_m}$ = 3,600 s (row VI), $\frac{1}{\eta_m}$ = 5,400 s (row VII), $\frac{1}{\eta_m}$ = 7,200 s (row VIII), and $\frac{1}{\eta_m}$ = 1,000 h (row IX). The black and dashed lines are the mean and SD of experimental data (n = 11). The red curves indicate the mean values over 10 simulations. (*A*) Time evolution of the pillar density (number of pillars per cm^2). (*B*) Time evolution of the average nearest-neighbor distance between pillars (mm). (*C*) Time evolution of the surface covered by the caps built over the pillars, as a fraction of the total surface and expressed in %. (*D*) Distribution of nearest-neighbor distances between pillars after 96 h. (*E*) Pair correlation function of the pillars positions.

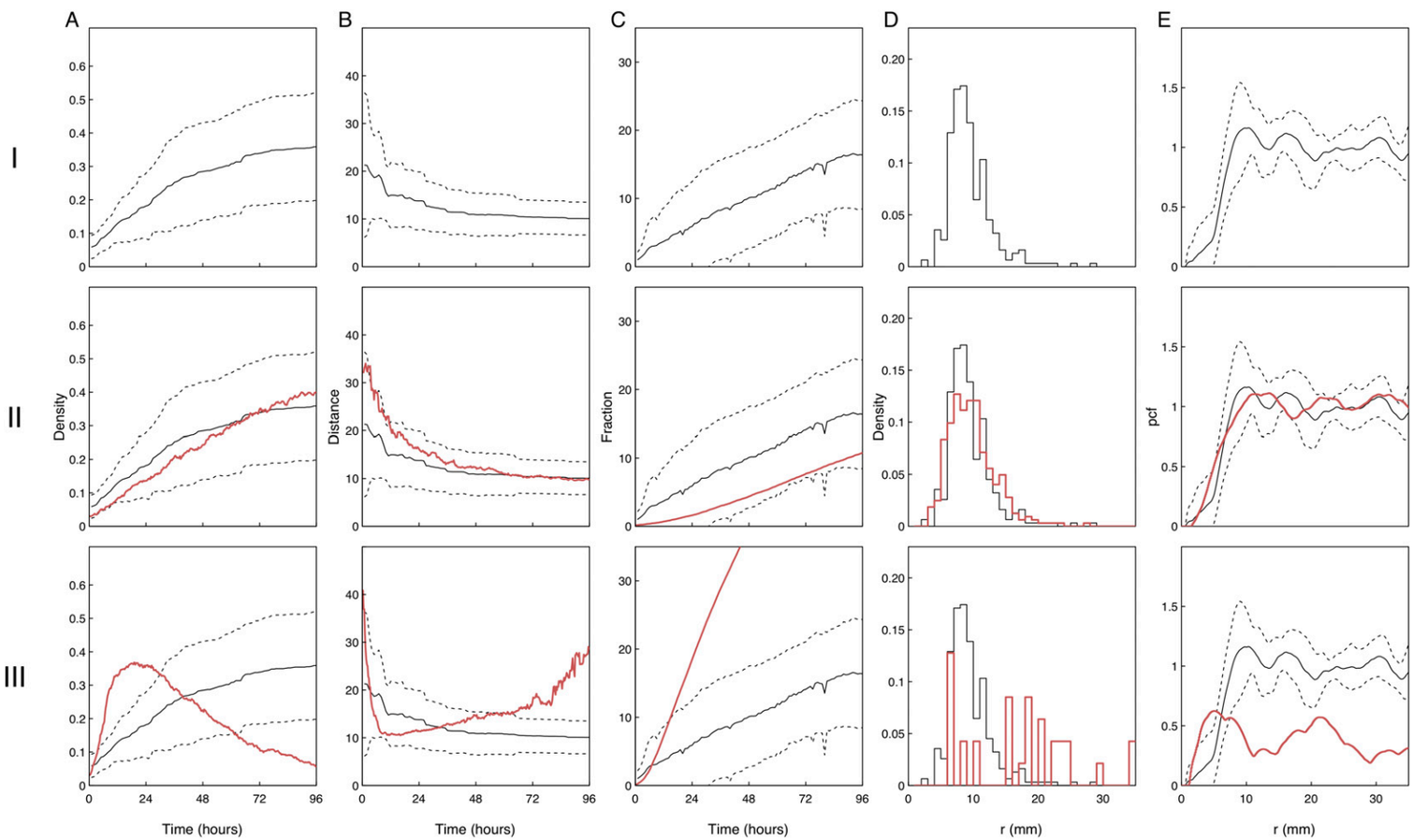

Fig. S9. Impact of the number of workers on the emerging spatial patterns: comparison between the observed and simulated data with pheromone mean life time $\frac{1}{\eta_m} = 1{,}000$ s and groups of 250 ants (row I), 500 ants (row II), and 1,000 ants (row III). The black and dashed lines are the mean and SD of the experimental data ($n = 11$). The red curves indicate the mean values over eight simulations. (*A*) Time evolution of the pillar density (number of pillars per cm^2). (*B*) Time evolution of the average nearest-neighbor distance between pillars (mm). (*C*) Time evolution of the surface covered by the caps built over the pillars, as a fraction (expressed in %) of the total surface. (*D*) Distribution of nearest-neighbor distances between pillars after 96 h. (*E*) Pair correlation function of the pillars' positions. The number of ants at work affects the building dynamics: with few workers, no pillars are built (thus no red lines in row I), whereas increasing the number of workers greatly accelerates the dynamics (rows II and III). The global rate of pellet picking-up per unit area is actually proportional to the density of workers and interacts with pheromone decay: if the global picking-up rate is too low (too few workers) (row I), pheromone decay dominates and no amplification of dropping can occur. When the picking-up rate is increased (rows II and III), pellet dropping is amplified and the pillar dynamics are accelerated. This process permits, in turn, a rapid transition to the extension of caps, which then fuse together (this explains the apparent decrease of the number of pillars in row III). We note however that the typical distance between pillars remains the same (10 mm, at 96 h in row II and at 24 h in row III). In short, emergence of the structures requires a minimal number of workers and it is accelerated when more workers are present.

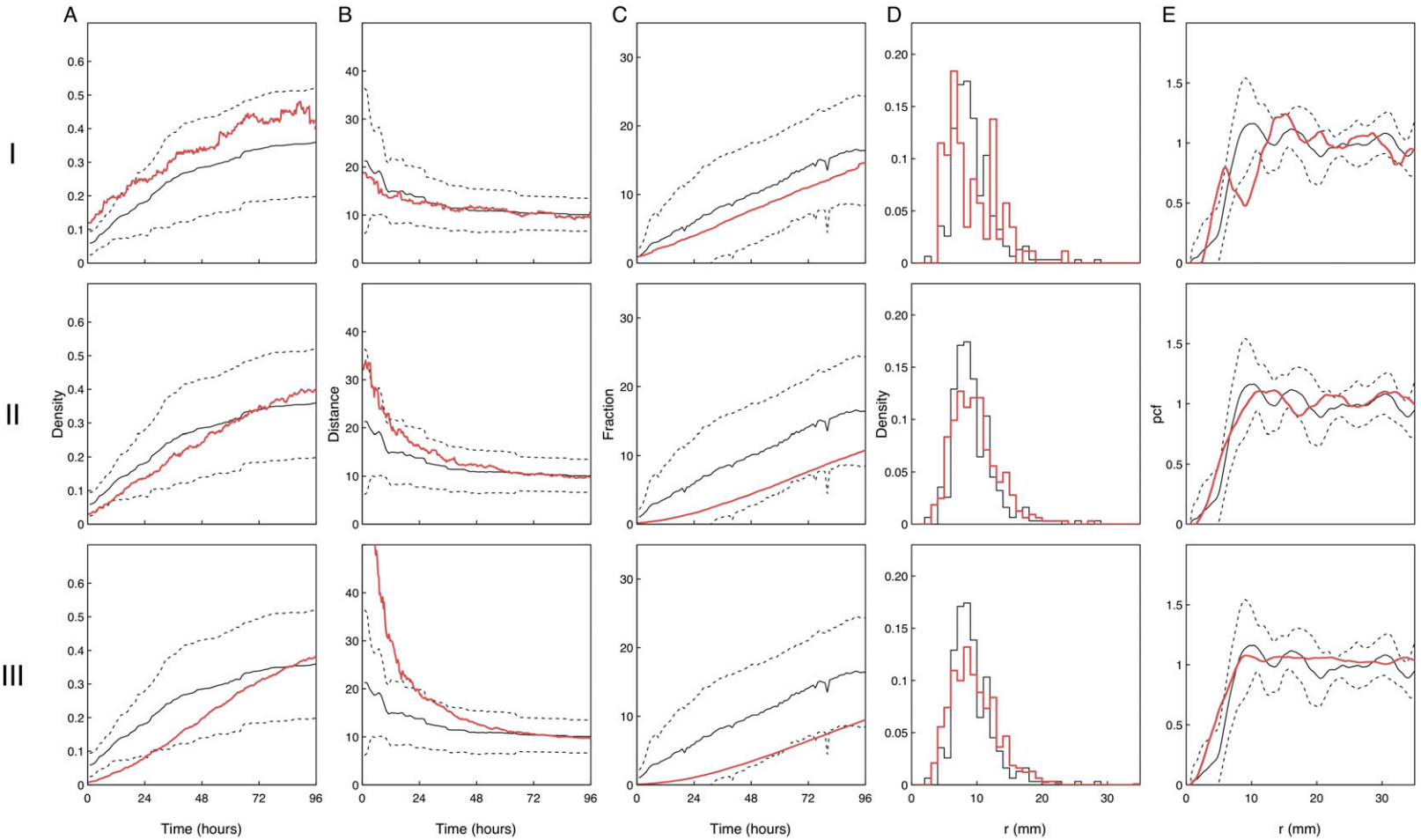

Fig. S10. Impact of the available area on the spatial patterns: comparison between the observed and simulated data with pheromone mean life time $\frac{1}{\eta_p}$ = 1,000 s. Row II corresponds to the experimental conditions (same as Fig. S9, row II), row I corresponds to an area four times smaller, and row III corresponds to an area four times larger. The black and dashed lines are the mean and SDs of the experimental data ($n = 11$). The red curves indicate the mean values over eight simulations. (*A*) Time evolution of the pillar density (number of pillars per cm^2). (*B*) Time evolution of the average nearest-neighbor distance between pillars (mm). (*C*) Time evolution of the surface covered by the caps built over the pillars, as a fraction (expressed in %) of the total surface. (*D*) Distribution of nearest-neighbor distances between pillars after 96 h. (*E*) Pair correlation function of the pillars positions. There is only a small effect of available area on the building dynamics: only the early dynamics of average nearest-neighbor distances seem to change significantly. This effect can be purely statistical: a larger area contains more pillars and elicits, in turn, a larger deviation toward large distances when the number of pillars is still low (in the beginning). Most importantly, the distribution of nearest-neighbor distances at 96 h (*D*) remains the same, indicating that the typical spatial wavelength of the pattern is not specific to the used experimental area.

Movie S1. Construction dynamics with a group of 500 ants over a period of 96 h. A large-scale regular pattern emerges from the individual building actions of ants. Pillars look like small columns that are topped by caps.

Movie S1

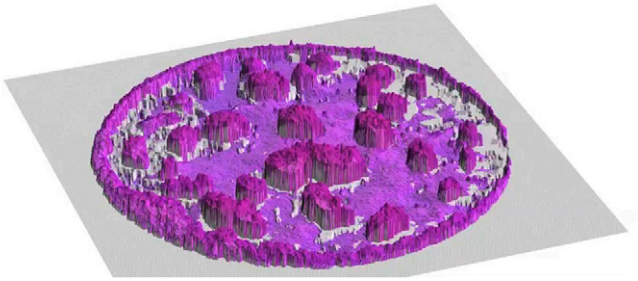

Movie S2. Three-dimensional video reconstruction of the built structures from laser scanner data over a period of 96 h.

Movie S2

Movie S3. Quantification of individual behavior. The red circle highlights a picking-up event, and the blue circle highlights a deposition event.

Movie S3

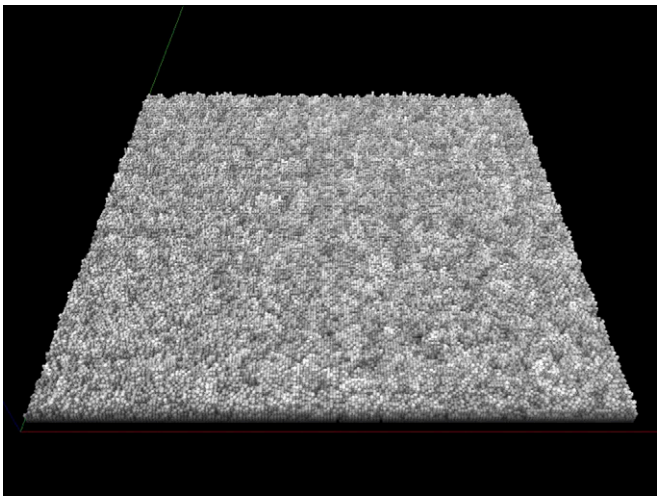

Movie S4. A typical run of the agent-based model with no pheromone, 500 ants, and $2 \cdot 10^5$ building particles. Other parameters are given in *Results*, and the total simulation time is 96 h.

Movie S4

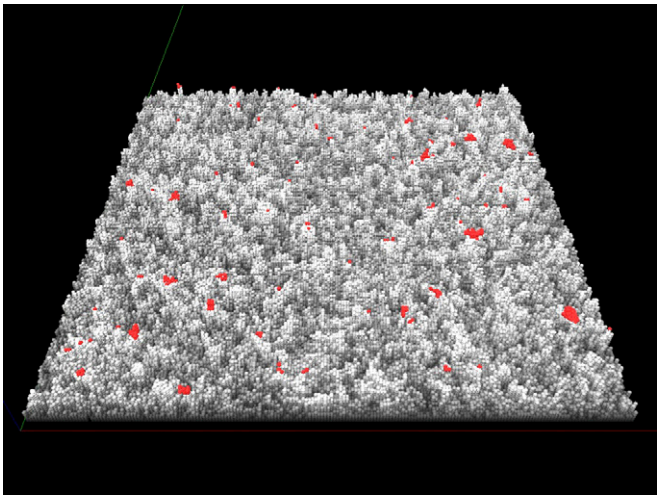

Movie S5. A typical run of the agent-based model for $\frac{1}{\eta_m} = 600$ s, 500 ants, and $2 \cdot 10^5$ building particles. Other parameters are given in *Results*, and the total simulation time is 96 h. The structures built above a height of 3 mm are represented in red.

Movie S5

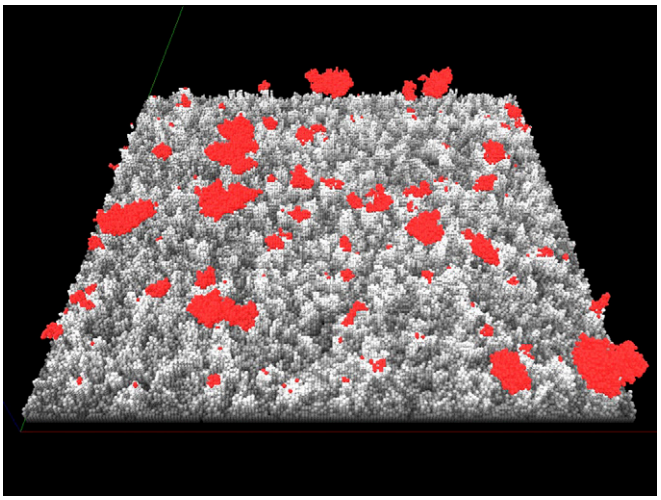

Movie S6. A typical run of the agent-based model for $\frac{1}{\eta_m} = 1{,}200$ s, 500 ants, and $2 \cdot 10^5$ building particles. Other parameters are given in *Results*, and the total simulation time is 96 h. The structures built above a height of 3 mm are represented in red.

Movie S6

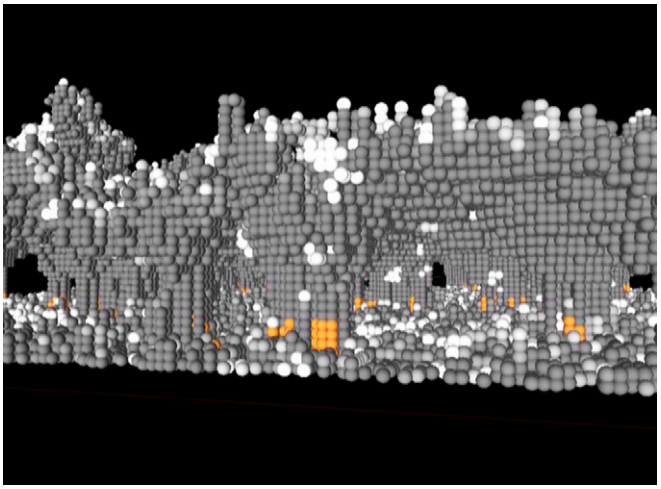

Movie S7. A close view of a simulation run of the agent-based model for $\frac{1}{\eta_m} = 1{,}200$ s, 500 ants, and $2 \cdot 10^5$ building particles showing the constant remodeling activity of the built structures.

Movie S7

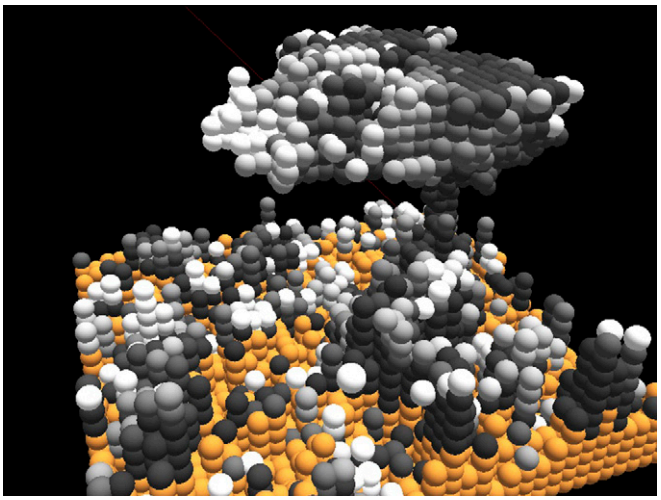

Movie S8. A close view of a simulation showing the complex topochemical landscape created by the heterogeneous amount of pheromone in the building pellets that compose the pillar. The gray scale indicates the amount of pheromone: the most recently deposited pellets are shown in light gray, and the oldest pellets are in dark gray.

Movie S8

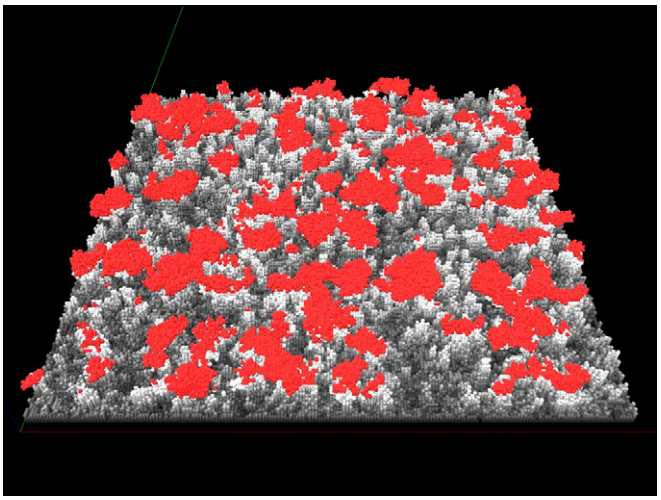

Movie S9. A typical run of the agent-based model for $\frac{1}{\eta_m} = 7{,}200$ s, 500 ants, and $2 \cdot 10^5$ building particles. Other parameters are given in *Results*, and the total simulation time is 96 h. The structures built above a height of 3 mm are represented in red.

Movie S9

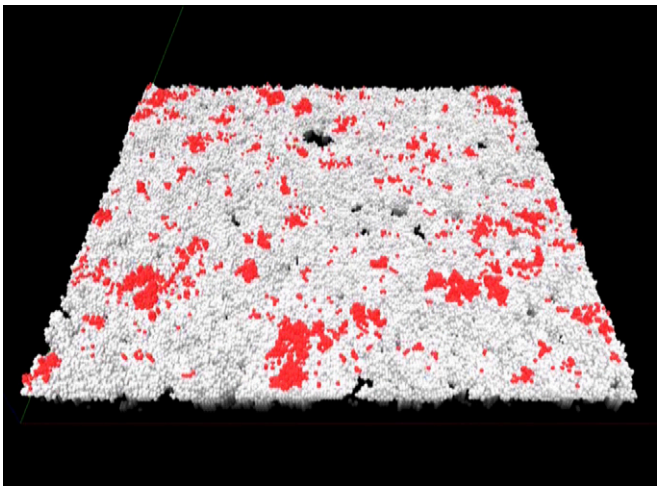

Movie S10. A typical run of the agent-based model for $\frac{1}{\eta_m} = 1{,}000$ h, 500 ants, and $2 \cdot 10^5$ building particles. Other parameters are given in *Results*, and the total simulation time is 255 d. The structures built above a height of 3 mm are represented in red.

Movie S10